INTERNATIONAL JOURNAL FOR NUMERICAL METHODS IN FLUIDS, VOL. 26, 39–56 (1998)

LOW-REYNOLDS-NUMBER FLOW AROUND A SQUARE CYLINDER AT INCIDENCE: STUDY OF BLOCKAGE, ONSET OF VORTEX SHEDDING AND OUTLET BOUNDARY CONDITION

A. SOHANKAR,[1] C. NORBERG[2] AND L. DAVIDSON[1]*

[1] *Thermo and Fluid Dynamics, Chalmers University of Technology, S-412 96 Göteborg, Sweden*
[2] *Division of Heat Transfer, Lund Institute of Technology, PO Box 118, S-221 00 Lund, Sweden*

SUMMARY

Calculations of unsteady 2D flow around a square cylinder at incidence ($\alpha = 0^\circ - 45^\circ$) are presented. The Reynolds numbers are low ($Re = 45$–200) so that the flow is presumably laminar. A von Kármán vortex sheet is predicted behind the cylinders with a periodicity which agrees well with experiments. An incompressible SIMPLEC code is used with a non-staggered grid arrangement. A third-order QUICK scheme is used for the convective terms. The time discretization is implicit and a second-order Crank–Nicolson scheme is employed. At the outlet of the computational domain a convective Sommerfeld boundary condition is compared with a traditional Neumann condition. The convective boundary condition is shown to be more effective in reducing the CPU time, reducing the upstream influence of the outlet and thus reducing the necessary downstream extent of the domain. A study of the effects of spatial resolution and blockage is also provided. The onset of vortex shedding is investigated by using the Stuart–Landau equation at various angles of incidence and for a solid blockage of 5%. A number of quantities such as Strouhal number and drag, lift and moment coefficients are calculated. © 1998 John Wiley & Sons, Ltd.

Int. J. Numer. Meth. Fluids, **26**: 39–56 (1998)

KEY WORDS: square cylinder; incompressible flow; laminar vortex shedding; angle of incidence; onset of vortex shedding; blockage; open boundary condition

1. INTRODUCTION

The flow around slender cylindrical bluff bodies has been the subject of intense research in the past, mostly by experiments but recently also by using numerical simulation. This flow situation is popular not only because of its academic attractiveness but also owing to its related technical problems associated with energy conservation and structural design. This type of flow is of relevance for many practical applications, e.g. vortex flowmeters, buildings, bridges, towers, masts and wires.

Under normal circumstances and when these bluff structures are exposed to cross-flow, there is a massive separated region downstream of the body. Owing to wake instabilities, a time-periodic oscillation develops at some critical onset Reynolds number Re_{cr}. This is the Bénard–von Kármán

Correspondence to: L. Davidson, Thermo and Fluid Dynamics, Chalmers University of Technology, S-412 96 Göteborg, Sweden

CCC 0271–2091/98/010039–18 $17.50

Received November 1996

instability.[1] The periodic phenomenon is referred to as vortex shedding, while the antisymmetric wake flow pattern is normally referred to as the Kármán vortex street. In the laminar régime, which usually persists up to Reynolds numbers of about 200, the vortex shedding is characterized by a very-well-defined frequency.

1.1. Problem under consideration

The flow configuration is depicted in Figure 1. A fixed two-dimensional square cylinder with side A is exposed at some angle of incidence α to a constant freestream velocity U_∞. Incompressible flow with constant fluid properties is assumed. The Reynolds number is defined as $Re = U_\infty d/\nu$, where d is the projected width of the cylinder in the streamwise direction, $d/A = \cos\alpha + \sin\alpha$ ($0^\circ \leqslant \alpha \leqslant 45^\circ$). All geometrical lengths are scaled with d. The scaling with d also applies to the Strouhal number $St = f_S d/U_\infty$, where f_S is the shedding frequency, and to all forces and moment coefficients. The vertical distance between the upper and lower walls, H, defines the solid blockage of the confined flow (blockage parameter $\beta = 1/H$). Velocities are scaled with U_∞ and physical times with d/U_∞. The pitching moment M is referred to the geometrical centre, with positive values in the clockwise direction. The origin of force co-ordinates is placed at the geometrical centre, with drag force D positive in the x-direction and lift L positive in the y-direction; see Figure 1. The base suction coefficient $-C_{pb}$ was calculated from the pressure at the intersection of the cylinder and the base centreline. The stagnation pressure coefficient C_{ps} was calculated at the mean point of primary attachment, i.e. at the time-averaged stagnation point.

The main objective of the present study is to provide reliable results from simulations of flow around square cylinders at incidence ($\alpha = 0^\circ - 45^\circ$) for different Reynolds number up to 200. Apart from discussions on general flow features and further aspects of grid dependence, particular emphasis is put on effects of blockage, effective outlet boundary conditions and the onset of vortex shedding.

1.2. Review

1.2.1. Experimental. A considerable amount of experimental data has been gathered for square cylinders with one side facing the flow. However, experiments on the detailed effects of the angle of incidence are much scarcer; see e.g. References 2 and 3 and reference cited therein. In all these studies the Reynolds numbers are relatively high, ranging from about 500 to 10^5. At Reynolds numbers relevant to this study, i.e. $Re \leqslant 200$, the only experimental results available in the open literature seem to be those in References 4–8, which are all for $\alpha = 0^\circ$. In References 6 and 7 St, C_D and $-C_{pb}$ are shown for Reynolds numbers from about 100 upwards. (St from about $Re = 70$), while

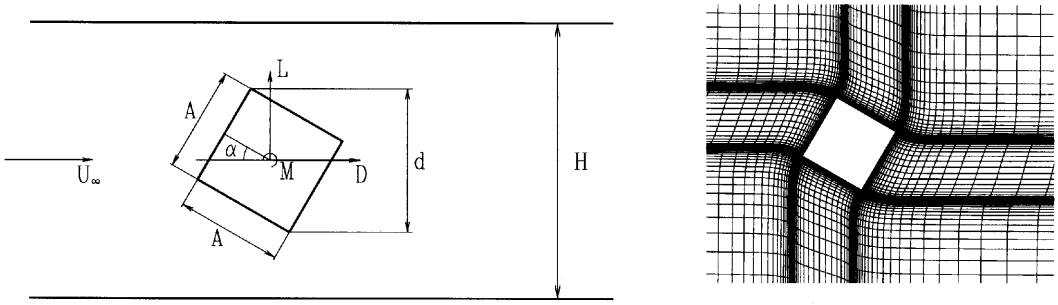

Figure 1. Flow configuration (left) and close-up of grid near cylinder (right)

in Reference 5 only *St* is shown for $Re \geqslant 200$. In addition, an $St - Re$ relationship for $Re \leqslant 400$ is provided by recent experiments of Norberg and co-workers.[8]

1.2.2. Numerical. For $Re \leqslant 500$ some relevant parameters from selected numerical investigations on 2D flow around a square cylinder are summarized in Table I. References 4, 9 and 10 use a $\psi\omega$ formulation, while the rest use primitive variables. For investigations on confined flow at high blockages see References 11 and 12. Note that in Reference 9, which apart from the present investigation is the only one covering arbitrary angles $\alpha = 0^\circ$–45°, the Reynolds number is calculated based on the side dimension A. For most investigations in Table I, i.e. References 8 and 13–16 as well as the present results, the upper and lower boundaries are treated as frictionless walls. In contrast, in References 5–7, 9 and 17 the upper and lower boundaries are assumed to be at the freestream condition.

In previous investigations the distance from the computational inlet to the cylinder, X_u in Table I, varies between $X_u = 4$ in References 15 to $X_u = 125$ in Reference 10. As shown in References 8 and 16, when using a freestream condition at the inlet, the necessary distance for obtaining results independent of this inlet location is about 10 units. For instance, as shown in Reference 16 for $Re = 100$, when X_u was increased from 7·5 to 11·1 units, there was a 9·3% decrease in RMS lift (the RMS lift is perhaps the best overall indicator when comparing results in vortex-shedding flows[8]). A further increase up to $X_u = 18$ gave negligible changes in the global results (less than 1%). For all investigations in Table I, except Reference 10, a freestream condition ($U = 1$, $V = 0$ or equivalent) is prescribed at the inlet.

Stegell and Rockliff[10] use a hybrid discrete vortex method in which the physical domain is approximately circular with a radius of 125 body diameters. A conformal transformation of the co-ordinate system is used in which the computational domain for solving the viscous diffusion equation is rectangular but periodic. The physical distance to the nearest grid point from the body at midspan is typically 0·03. At the outer radius of the physical domain the streamfunction ψ is set to its rotational flow value and the change in vorticity ω due to viscous diffusion is set to zero (Nathan Stegell, personal communication, 1996).

Table I. Two-dimensional simulations for square cylinder in uniform cross-flow ($Re \leqslant 500$)—summary of computational parameters: H, height of computational domain; X_u, distance from body to inlet; X_d distance from body to outlet; NM, numerical metod (FD, finite differences, FV, finite volumes; DV, discrete vortex); N, non-uniform; U, uniform

Reference	Year	*Re*	$\alpha(^\circ)$	H	X_u	X_d	Δt	NM	Grid
18, 4	1978/1982	150, 250	0	17	21·9	96·7	0·031	FD	N
5	1982	⩾100	0	12	4·5	9·5–14·5	0·05	FV	N
		250	5, 15	12	4·5	9·5–14·5	0·05	FV	N
19, 6	1987/1990	100, 150, 500	0	11	5	21	0·01	FD	N
13	1990	40–300	0	12	4·5	14·5	0·025 (0·012)	FV	N
14	1991	100, 500	0	13	5	15 (25)	0·02–0·03	FV	N
15	1992	100	0	7	4	9	0·125	FV	N
17	1993	100	0	16	7·5	19·5, 59·5	0·01	FD	U
9	1994	50–250	0	10	5	15	?	FD	U
		5–50	0–45	10	5	15	?	FD	U
16	1995	45–250	0	14–50	7·5–18	10–56	0·02–0·05	FV	N
8	1996	200	0–45	20	10,20	26, 40	0·025 (0·0125)	FV	N
10	1996	200	0	125	125	125	0·0035	DV	N
Present		45–200	0–45	20 (40)	10	3–26	0·025	FV	N

In numerical simulations of flow around bluff bodies, only a few investigations concerning parameters such as blockage, upstream/downstream extent, time step, grid resolution and boundary conditions are found. In each of those studies, only some of these aspects are investigated and no investigation has been found which extensively covers all these aspects.

For example, the effect of blockage is investigated numerically in References 20–22 for circular cylinders ($Re \leqslant 180$) and in Reference 16 for square cylinders ($Re = 100$). It is shown that with increasing blockage parameter β the Strouhal number and drag coefficient increase, while the base suction and stagnation pressure coefficients increase. At high Reynolds numbers this is also observed experimentally for rectangular cylinders, circular cylinders and flat plates.[23–25] Some further effects of blockage are provided in Section 4.2.

The influence of domain size, especially the location of the outflow boundary, X_d in Table I, is investigated in References 16 and 26 for $Re = 100$ and in Reference 8 for $Re = 200$. Behr *et al.*[26] consider the flow around a circular cylinder using a ψ–ω formulation and by applying two types of outlet boundary conditions. It is shown that if X_d is selected less than 2·5 diameters from the body, then the temporal periodicity of the solution is lost. The minimum value of X_d is found to be 6·5. It is also concluded that reliable results for both types of boundary conditions are obtainable with $X_d = 14{\cdot}5$. In Reference 16 the influence of X_d between 10 and 56 is investigated ($Re = 100$) using the standard Neumann condition at the outlet (hereafter referred to as the NBC). The results indicate that in order to obtain results independent of the outlet, X_d must be larger than about 20. Further investigations in Reference 8 confirm this suitable extent also for $Re = 200$. It is believed that this seemingly large discrepancy in the suitable value of X_d is due to the actual type of outlet boundary condition used. Obviously, in these vortex-shedding flows, the distance from the cylinder to the outlet (X_d) is a parameter of special importance. This matter will be pursued further in Section 2.1.

Some refinement studies are carried out in References 8, 13, 14 and 16. Franke *et al.*,[13] who consider both circular and square cylinders, present some limited studies with different time steps and near-wall resolutions. They conclude that the distance of the first grid point away from the body (δ) has a strong influence on the results. For flow around square cylinders at $Re = 100$ and 200 they used $\delta = 0{\cdot}0038$ and 0·0013 respectively ($\Delta t = 0{\cdot}025$ and 0·012). A grid refinement study for flow around a square cylinder at $Re = 500$ is presented by Arnal *et al.*[14] They employ three grids (119×137, 60×69 and 40×45) and report some significant grid dependences. For example, the RMS lift was decreased three times when going from the finest to the coarsest grid. In previous work of Sohankar *et al.*[16] for a square cylinder at zero incidence the effects of time step, distribution of grid points, size of cells adjacent to the body, upstream and downstream extents of the calculational domain and blockage are thoroughly investigated ($Re = 100$). The influence of Reynolds number ($Re = 45$–250) at blockage $\beta = 5\%$ is also presented. In that study, when using a highly non-uniform grid, some recommendations for the required size of the domain, grid distribution, time step and spatial resolution in the near-body region are provided. In recent work of Sohankar *et al.*[8] for rectangular cylinders with side ratios $B/A = 1, 2, 4$ at incidence ($\alpha = 0^\circ$–90°) and $Re = 200$, special emphasis was put on factors such as time and spatial resolution, grid dependence, influence of domain size, general flow features for laminar vortex-shedding flows and effects of angle of incidence and side ratio. In that study it is concluded that the results may be strongly dependent on the spatial resolution in both the far and near fields. Grid refinement studies are provided in Section 4.3.

2. NUMERICAL DETAILS

The flow is assumed to be two dimensional and unsteady. An incompressible SIMPLEC finite volume code is used with a non-staggered grid arrangement. The scheme is implicit in time and a Crank–Nicolson scheme of second order has been used for convective and diffusive terms; the pressure is

treated fully implicitly. The convective terms are discretized using the third-order QUICK differencing scheme, while the diffusive terms are discretized using central differences. More details of the code, equations, etc. are given in Reference 8.

The time-marching calculations are started with the fluid at rest. A constant time step $\Delta t = 0{\cdot}025$ is used for all calculations. During the iterative sequence, convergence is assessed at the end of each iteration on the basis of the residual source criterion, which compares the sum of the absolute residual sources over all the control volumes in the computational field, for each finite volume equation. The residuals for the continuity and momentum are normalized with the incoming mass flux and momentum flux in the x-direction respectively. The convergence criterion is set to 0·001. Tests with a convergence criterion of 0·0001 and double precision show no significant changes in the results (e.g. less than 0·5% for the RMS lift), while the number of iterations to convergence increases approximately two times.

Outside a region from the body which extends 5 units upstream, downstream and sideways, the grid distribution was made uniform with a constant cell size Δ. However, for refinement cases ($\Delta \leqslant 0{\cdot}15$) the corresponding grid non-uniform extension was instead 2 units.

The distance from the cylinder surface to the nearest grid point defines δ. For all calculations in this paper, $\delta = 0{\cdot}004$. The hyperbolic tangent function was used for stretching the cell sizes between these limits (δ and Δ); see Figure 1. The number of nodes distributed over unit length of the cylinder surface is denoted N_b. Unless stated otherwise, the following values apply: $\Delta = 0{\cdot}5, N_b = 20$.

2.1. *Boundary conditions*

One of the chief difficulties encountered in numerical solution of the Navier–Stokes equations is that of boundary conditions, especially the outflow boundaries. This difficulty is due to the fact that the computational domain is bounded whereas the physical domain is unbounded. Thus the computational domain should be truncated from the real domain by using artificial open boundary conditions such as Neumann (NBC) or convective (CBC) boundary conditions. For high accuracy the computational domain must sometimes be very large and this increases CPU times and the cost of computation. Thus proper boundary conditions can reduce the size of the computational domain and decrease the cost. In most numerical studies, especially those which involve vortex shedding, the outlet (open) boundary condition is a very important issue.

A suitable outflow boundary (i) permits the flow to exit the domain with a smooth discharge of vortices, (ii) has a minimum effect on the flow in the domain near the outlet and finally (iii) has a negligible effect on the near-body flow. Incorrect location of outflow boundaries and non-suitable boundary conditions might seriously affect the whole flow structure, especially near the body.

For finite difference and finite volume discretizations the NBC and CBC are the two most popular outlet boundary conditions. For example, all the studies in Table I, except References 5, 9 and 14, use an NBC. Arnal *et al.*[14] use a CBC, while Davis and Moore[5] employ the momentum equation at the outlet by ignoring the diffusion terms and employing first-order upwind differencing of the convective terms for the computation of the velocities. Zaki *et al.*[9] set the second and first derivatives of the streamfunction and vorticity equal to zero at the outlet.

The particular issue of outflow boundary conditions for flow around a square cylinder is investigated by Yoshida *et al.*[17] For $X_d \approx 20$ and 60 they compare four types of open boundary conditions, namely an NBC and three kinds of CBC. The NBC produced significant deformations of the outlet velocity and pressure fields, while the type of CBC utilizing the freestream velocity was found to have the least influence. However, results for global parameters such as Strouhal number and drag and lift coefficients were more or less unaffected by the outlet condition.

In previous work of the authors,[16] using an NBC at $Re = 100$ and $\alpha = 10^\circ$, it is shown that when the downstream extent X_d is not sufficiently large, i.e. when $X_d < 20$ approximately, the global flow pattern is affected, causing significant changes in the results. In this study we extend that investigation by using a CBC in a form which has previously been shown to be well suited for unsteady vortical flow structures moving out of the computational domain.[17,27]

On reviewing the literature, it is evident that many types of outlet boundary conditions have been used in the context of vortex-shedding flows. For instance, the second derivative of any dependent variable at the outlet might be set equal to zero. As reported by Arnal *et al.*,[14] this boundary condition might lead to numerical instabilities with diverging results. When testing this condition, some similar instabilities were observed in the present investigation. Sometimes, vanishing third-order streamwise derivatives of the velocity and pressure at the outlet are used; see e.g. Reference 28. Further information about different types of boundary conditions can be found in References 29–35.

In general the CBC can be written for both U and V as

$$\frac{\partial U_i}{\partial t} + U_c \frac{\partial U_i}{\partial x} = 0,$$

where U_c is the convective velocity/phase speed ($U_1 = U$, $U_2 = V$). In References 17, 27 and 36, the CBC is tested with both variable and constant (uniform) velocity, with negligible differences in the statistical results. Thus in this study, as also recommended in Reference 17, the value of U_c was set to U_∞. The discretized form of this equation was implemented as

$$U_N^* = U_N^n - \frac{\Delta t}{(\Delta x)_N} U_c (U_N^n - U_{N-1}^n), \qquad U_N^{n+1} = U_{cor} + U_N^*,$$

where the superscript denotes the time level and the index N refers to the streamwise grid number at the outlet. U_{cor} is a correction velocity to guarantee the balance between mass inflow and outflow (computed from U_N^*) at each iteration. The correction velocity, which is constant over the entire outlet, is obtained from the difference between mass inflow and outflow and is zero at the end of each time step when convergence is reached.

In this study the following boundary conditions were used. At the inlet, which is located $X_u = 10$ units upstream of the most upstream corner of the cylinder, a uniform flow was prescribed ($U = 1$, $V = 0$). At the outlet, which is located X_d units downstream of the most downstream corner, an NBC and a CBC for both U and V were used. No-slip conditions were prescribed at the body surfaces. At the upper and lower boundaries, symmetry conditions simulating a frictionless wall were used ($\partial U/\partial y = V = 0$). The second normal derivatives for the pressure was set to zero at all boundaries.

3. ONSET OF VORTEX SHEDDING

For cylindrical structures with non-streamlined forebodies and short afterbodies (e.g. a square cylinder) the critical Re, when scaled with the cross-stream dimension d, is $Re_{cr} \approx 50$; see References 8, 15, 37 and 38. As shown by e.g. Provansal *et al.*,[1] Schumm *et al.*[38] and Park,[39] the onset from steady to periodic flow is characterized by a Hopf bifurcation which can be described by the Stuart–Landau equation

$$\frac{dC}{dt} = \sigma C - l|C|^2 C, \tag{1}$$

where $C(t)$ is a characteristic complex amplitude associated with the fundamental frequency component, $\sigma = \sigma_r + i\sigma_i$ is the linear growth rate and $l = l_r + il_i$ is the first Landau 'constant' (for a

supercritical bifurcation, $l_r > 0$).[38] After linearizing the real part of equation (1) around Re_{cr}, where $\sigma_r = 0$, the instantaneous growth rate at $Re > Re_{cr}$ is

$$S = |C|^{-1}\frac{d|C|}{dt} = \sigma_r - l_r|C|^2 = \sigma_r\left(1 - \frac{|C|^2}{|C|^2_{sat}}\right), \tag{2}$$

where $|C|_{sat}$ is the envelope amplitude in the saturated state. To first order, at small departures from onset the real part of σ_r is a linear function of $Re - Re_{cr}$, i.e.

$$\sigma_r = K(Re - Re_{cr}), \tag{3}$$

where K is a positive constant.

Strictly speaking, equations (2 and 3) are valid only at Re very close to onset. Based on experimental observation (see Reference 38), however, they seem to be applicable for $Re - Re_{cr}$ ranging from -10 to 20 approximately. From transient real measurements or numerical simulations at Reynolds numbers close to onset, yielding different values of σ_r (using viscous time scaling), the onset value Re_{cr} is determined in equation (3) by interpolation. In the present study the function C, as in Reference 39, was chosen to be the lift coefficient, i.e. $C_r = C_L$. In this respect, as mentioned in Reference 38, the analysis relies on the fact that the linear growth rate is independent of location, i.e. vortex shedding results from a time-amplified global instability.[1] The onset may also be studied by applying linear stability analysis to autonomous dynamical systems.[15,37,40,41] As also mentioned in Reference 38, the vortex shedding during start-up is always two-dimensional. Thus a two-dimensional method for prediction of the onset of vortex shedding is suitable.

4. RESULTS AND DISCUSSION

An investigation of the influence of computational parameters such as far-field resolution, blockage and domain sizes and outlet boundary condition as well as the influence of onset of vortex shedding, Reynolds number and angle of incidence was performed. In the fully staturated state, i.e. at physical times when memory effects of the starting process are negligible, many useful physical quantities were computed, e.g. the dominating wake frequency (Strouhal number), mean and RMS values for various wall pressures as well as body lift, drag and moment coefficients.

4.1. Outlet boundary condition

A study of the influence of the two common outlet boundary conditions NBC and CBC was performed and the results are compiled in Table II and Figures 2–4. In Figure 2, for $Re = 200$ and $\alpha = 0^\circ$, the time-averaged pressure coefficient C_p along the centreline is depicted for various locations of the outlet boundary using both the NBC and CBC. Further comparisons for this flow case are shown in Figure 3 (effects on time-averaged pressure and vorticity contours) and in Figure 4 (effects on the number of iterations per time step during the time-dependent simulation).

For the NBC cases a pronounced dip in the centreline C_p was present near the outlet (Figure 2, left); see also Reference 16. Evidently, this distortion was much less when using the CBC (Figure 2, right). In addition, when X_d is not sufficiently large, the global flow pattern is seriously affected (Figure 3), causing significant changes in both pressure and vorticity around the body. However, the minimum X_d for negligible near-body effects is much lower with the CBC than with the NBC. It is important to point out, however, that if X_d is sufficiently large, regardless of the outlet condition (NBC or CBC), the upstream influence from the outlet is effectively damped out. As an example, on comparing cases 1 and 2 in Table II, both with $Re = 100, \alpha = 0^\circ$ and the NBC, there is an 83% decrease in the RMS lift on going from $X_d = 26$ to $X_d = 10$. In contrast, case 3 in Table II, also with

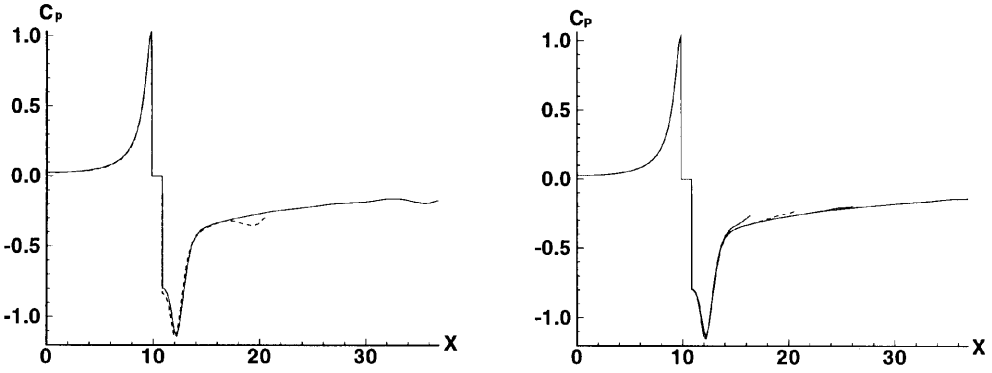

Figure 2. Comparison of time-averaged pressure coefficient along centreline for NBC (left; $X_d = 10, 26$) and CBC (right; $X_d = 5{\cdot}5, 10, 15, 26$) at $Re = 200$

$Re = 100$ and $\alpha = 0^\circ$ but now with the CBC and $X_d = 10$, essentially has the same global results as the NBC with $X_d = 26$ (case 1).

On comparing results in Table II for the NBC ($X_d = 26$) and CBC ($X_d = 10, 15, 26$), the overall difference is about 1%. Thus, by selecting the CBC, the suitable size of X_d may be as low as 10 (as compared with about $X_d = 25$ with the NBC[16]). Evidently (see Figure 3), the flow using the CBC exits the domain with a smooth discharge of vortices, with only a small local effect on the outlet flow, especially for $X_d \geqslant 10$ where the near-body flow is virtually unaffected.

It is important to emphasize that the suitable value of X_d depends on the Reynolds number. At lower Reynolds number the viscous diffusion, and consequently the formation length of the recirculating region behind the body (L_r), is larger. The maximum value of L_r occurs at around the onset of vortex shedding.[16,42] For example, in the present study the time average of L_r was calculated to be 3·69, 2·20 and 1·67 for $Re = 50$, 100 and 200 respectively. Thus at low values of X_d, especially with the NBC, this near-wake flow might be seriously affected, leading to detrimental effect on the global results. With the CBC the flow patterns and global results start to deviate from the outlet-independent flow at around $X_d = 10$; see Figure 3. For instance, on decreasing X_d from 10 to 5·5, there was an increase of about 5% in the RMS lift. The influences on the global results became unacceptable for smaller values of X_d, for example, on decreasing X_d from 10 to 3, the changes in Strouhal number, RMS lift and base suction coefficient were $-8{\cdot}9\%$, 6·5% and 6·8% ($Re = 100$) and $-10{\cdot}3\%$, 29% and -5% ($Re = 200$) respectively (Table II). Thus it seems that the location of the outlet boundary with the CBC must be in the region where the gradients of pressure and velocity are small (Figure 2). In summary, for the CBC the suitable value of X_d seems to be 10 units. However, for safety we recommend 15 units, especially at $Re < 100$ for which the recirculating region behind the body is larger and the flow more viscous.

The NBC generates disturbances in the upstream flow which evidently are damped out rather slowly. This causes the number of iterations per time step, N_{it}, to increase, especially when compared with the CBC; see Figure 4. In Table II the average number of iterations per time step in the saturated condition of vortex shedding, N_p, and the average number of iterations per time step for the whole simulation, N_t (6300 and 4300 time steps for $Re = 100$ and 200 respectively), are provided. As these numbers are measures of the CPU time of calculation, there was a significant saving in CPU time on going from the NBC to the CBC, at least for the case at zero incidence. In addition, the CBC causes an earlier transition to fully periodic saturated flow; see Figure 4. In other words, the CBC in comparison with the NBC saves CPU time in three different ways: (i) by decreasing the number of

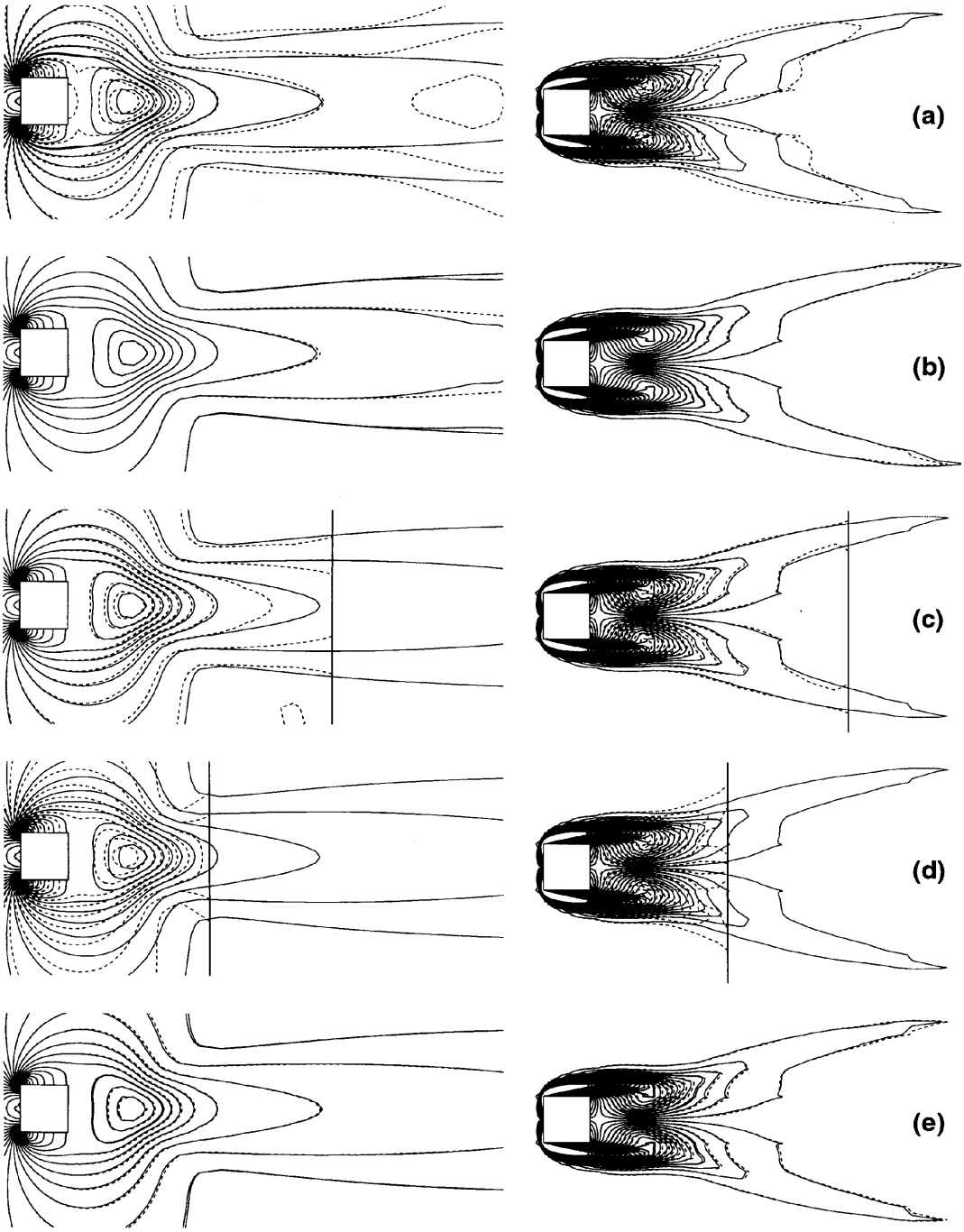

Figure 3. Comparison of time-averaged pressure (left; $\Delta C_p = 0{\cdot}1$) and vorticity (right; $\Delta\omega = 0{\cdot}2$) at $Re = 200$: (a) NBC ($X_d = 10, 26$); (b) CBC ($X_d = 10, , 26$; (c) CBC ($X_d = 5{\cdot}5, 10$); (d) CBC ($X_d = 3, 10$); (e) NBC ($X_d = 26$) and CBC ($X_d = 10$). Broken lines correspond to $X_d = 10$ in (a), (b) and (e), to $X_d = 5{\cdot}5$ in (c) and to $X_d = 3$ in (d)

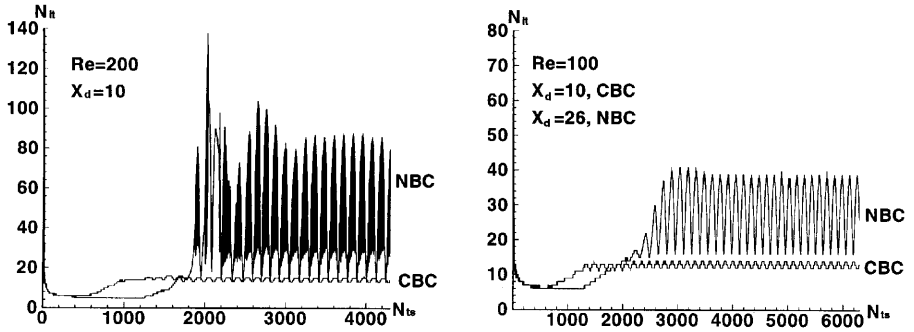

Figure 4. Time evolution of number of iterations per time step for different outlet boundary conditions ($Re = 200$, $\alpha = 0^\circ$). N_{ts} is the time step number

iterations for convergence in each time step (up to about 50%), (ii) by decreasing the CPU time for each iteration owing to reduced X_d (by about 25% on changing X_d from 26 to 10) and finally (iii) by decreasing the time to reach fully periodic flow.

By comparing cases 13 and 14 in Table II, it is found that the CBC is also suitable for flow around a square cylinder with non-zero angle of incidence. As can be seen, the difference between the results is less than 1%. Interestingly, it is found that the NBC works better in cases with flow incidence ($\alpha \neq 0^\circ$). This may be a result of the fact that these cases had a stronger and more vigorous vortex shedding as compared with zero incidence (e.g. for $Re = 200$, where the RMS lift at $\alpha = 30^\circ$ was three times higher than at $\alpha = 0^\circ$). The numerical disturbances generated by the NBC could then be damped out more effectively.

It is important to emphasize that most of these differences in results and flow patterns for different boundary conditions were not observed when X_d was selected large (e.g. $X_d = 26$). This is also evident from the results of Yoshida *et al.*[17]

4.2. *Influence of blockage*

In previous work of the authors[16] for a square cylinder at zero incidence the blockage effect was investigated for $Re = 100$ and $\Delta = 0{\cdot}7$ by using two different schemes for the convective terms

Table II. Effect of outlet boundary conditions

Case	Re	α	BC	X_d	St	C_D	C_{D_p}	$C_{L'}$	$-C_{pb}$	C_{ps}	N_t	N_p
1	100	0	NBC	26	0·147	1·464	1·418	0·138	0·663	1·052	22·8	28·7
2	100	0	NBC	10	0·150	1·491	1·441	0·024	0·691	1·051	32·8	40·3
3	100	0	CBC	10	0·146	1·460	1·414	0·139	0·661	1·052	13·5	12·9
4	100	0	CBC	5·5	0·145	1·452	1·407	0·146	0·661	1·053	13·0	12·3
5	100	0	CBC	3	0·133	1·426	1·382	0·148	0·616	1·052	10·8	10·9
6	200	0	NBC	26	0·167	1·439	1·480	0·227	0·797	1·030	24·2	35·9
7	200	0	CBC	26	0·167	1·428	1·469	0·228	0·797	1·034	15·9	13·8
8	200	0	CBC	15	0·165	1·428	1·468	0·229	0·793	1·034	15·4	13·1
9	200	0	NBC	10	0·167	1·465	1·504	0·240	0·837	1·028	28·8	38·3
10	200	0	CBC	10	0·165	1·427	1·467	0·232	0·792	1·034	15·1	13·1
11	200	0	CBC	5·5	0·165	1·431	1·471	0·241	0·796	1·035	14·6	13·0
12	200	0	CBC	3	0·148	1·398	1·438	0·301	0·752	1·037	13·3	11·5
13	200	30	NBC	26	0·203	1·899	1·729	0·728	1·535	1·044	18·6	16·2
14	200	30	CBC	10	0·203	1·905	1·724	0·728	1·544	1·050	18·0	15·9

(QUICK, Van Leer). In that study it is reported that the calculations exhibit unphysical oscillations for a blockage of less than 3% when using the QUICK scheme. For reduction of truncation errors and numerical diffusion, which are more sever in non-uniform grid simulations, the recent work of the authors[8] as well as this study highlights the special important of a suitable grid distribution and a fine enough far-field resolution. In this study, by decreasing the blockage to 2·5% for different Reynolds numbers, the effect of blockage was investigated and results are compiled in Table III. Since both the grid distribution and far-field resolution were changed in this study in comparison with Reference 16, we could not detect any unphysical oscillations in the present calculations.

On changing the blockage parameter from $\beta = 5\%$ (see Table III), the strongest effects occurred for the base suction coefficient $-C_{pb}$. For $Re = 100$, 150 and 200 the decrease in base suction was 7·6%, 5.4% and 5·0% respectively. The corresponding changes in other quantities were rather small (less than 3%). For instance, the maximum decrease in Strouhal number was 1·4%, which occurred for $Re = 100$. For the square cylinder at these rather low values of Re we could not find any previous study with which to make a direct comparison. However, there are some investigations for other geometries. For example, Behr *et al.*[22] investigate the effect of blockage for a circular cylinder ($Re = 100$). Their results show that on decreasing the blockage from $\beta = 5{\cdot}5\%$ to 1·6%. St, C_D and C_L decrease by 5%, 6% and 6% respectively. Similar behaviour can be seen in the other investigations of blockage; see e.g. References 16 and 20–25.

In summary, on decreasing the blockage for different Reynolds numbers in the range $Re = 100 - 200$, St, C_D, C_{D_p} and $-C_{pb}$ decrease, while the stagnation pressure increases. These changes are all similar to a decrease in the Reynolds number corresponding to the fact that an increase in blockage is effectively an increase in the oncoming velocity.

4.3. Grid dependence

In recent work of the authors[8] an extensive study of various computational parameters is presented. At least for the non-uniform grids employed in that investigation and for such low-Reynolds-number vortex-shedding flows, the most crucial parameters for producing grid-independent results seem to be the far-field resolution Δ and the number of nodes distributed along unit length of the body, N_b. In this study, by using the CBC, the domain of calculation could be drastically reduced and the procedure of convergence is faster. These advantages now enable us to use even finer and more uniform grids, which are factors which will further reduce truncation errors and effects of numerical diffusion.

In Table IV, results are shown for different Δ down to 0·1. Cases 2 and 5 are taken from Reference 8 (C_{ps} and $-C_{pb}$ were not calculated in that study, hence the missing values in the table). For $Re = 200$, on decreasing Δ for 0·5 to 0·1, St, C_D, C_{D_p}, $C_{L'}$, $-C_{pb}$ and C_{ps} change by about $-9{\cdot}0\%$, 2·5%. 2·6%, 64%, 4% and 0·8% respectively. The majority of these differences occur on going from $\Delta = 0{\cdot}5$ to 0·25. Between $\Delta = 0{\cdot}15$ and 0·10, except for $C_{L'}$, which changes by 2·7%, the changes in

Table III. Blockage effect study for different Reynolds numbers at $\alpha = 0^\circ$

Case	Re	β(%)	Grid	St	C_D	C_{D_p}	$C_{L'}$	$-C_{pb}$	C_{ps}
1	200	5·0	96×94	0·165	1·427	1·467	0·232	0·792	1·034
2	200	2·5	96×132	0·165	1·415	1·455	0·229	0·752	1·060
3	150	5·0	96×94	0·162	1·417	1·429	0·160	0·721	1·040
4	150	2·5	96×132	0·160	1·400	1·411	0·166	0·682	1·067
5	100	5·0	96×94	0·146	1·460	1·414	0·139	0·661	1·052
6	100	2·5	96×132	0·144	1·444	1·399	0·141	0·611	1·083

Table IV. Refinement study at $\alpha = 0^\circ$

Case	Re	Δ	N_b	BC	X_d	Grid	St	C_D	C_{D_p}	$C_{L'}$	$-C_{pb}$	C_{ps}
1	100	0·50	20	CBC	10	96×94	0·146	1·460	1·414	0·139	0·661	1·052
2	100	0·30	20	NBC	26	191×141	0·146	1·477	1·433	0·156	—	—
3	100	0·15	40	CBC	10	210×202	0·146	1·478	1·434	0·153	0·678	1·059
4	200	0·50	20	CBC	10	96×94	0·165	1·427	1·467	0·232	0·792	1·034
5	200	0·25	30	NBC	26	348×224	0·149	1·445	1·488	0·360	—	—
6	200	0·15	40	CBC	10	210×202	0·150	1·466	1·507	0·367	0·829	1·040
7	200	0·10	40	CBC	10	284×274	0·150	1·462	1·505	0·377	0·825	1·042

the other quantities are negligible. For $Re = 100$, on decreasing Δ further below 0·3, the difference between results is negligible. For this range of Reynolds numbers, $Re \leqslant 200$, it is recommended that the cell Reynolds number, i.e. the Reynolds number based on Δ, should be less than 30.

4.4. Onset of vortex shedding

Within the full range of possible incidences, $0^\circ \leqslant \alpha \leqslant 45^\circ$, the simulations indicated the onset to occur within the interval $40 < Re_{cr} < 55$. By using the linearized Stuart–Landau equation as outlined in Section 3, for some selected angles of incidences within this interval the actual onset values were predicted. In this separate study both time and frequency were non-dimensionalized using the viscous time scale d^2/ν, where ν is the kinematic viscosity. The shedding frequency scaled in this way is usually referred to as the Roshko number

$$Ro = f_S d^2/\nu = Re \times St. \tag{4}$$

The following procedure was employed for finding Re_{cr}. As mentioned earlier (Section 3), the lift coefficient was selected as the raw signal in the analysis; see Figure 5(a). For each selected angle of incidence and each Re close to onset the value of σ_r was found from equation (2) by fitting a straight line in a plot of the non-dimensional instantaneous growth rate S versus the ratio $|C|^2/|C|^2_{sat} = R$; see Figure 5(b). The critical Reynolds number was then simply found from the location of $\sigma_r = 0$ after fitting, according to equation (3), a straight line in a plot of σ_r versus Re; see Figure 5(c). Note that for Re below onset the growth rate is negative. For some cases, e.g. for $Re = 50$ and $\alpha = 0^\circ$ (see Figure 5(c)), these values could be extracted from the simulations also. In these cases the disturbances from the start-up process caused shedding to commence for a short period of time.[16] Eventually, since Re was below onset, the shedding faded away (with a negative growth rate).

The critical Reynolds numbers are plotted in Figure 5(d). As is evident from Figure 5, the procedure did not always produce perfect fits. Moreover, at each angle of incidence the number of Re cases which could be analysed was rather small, only three to four. This means that the values of Re_{cr} found from the analysis have to be tagged with uncertainty intervals. The uncertainty was estimated to be $\pm 2\%$, corresponding to ± 1 for each Re_{cr}. It is important to mention that the simulations with the flow starting from rest will eventually certify whether the simulated Reynolds number is actually blow or above the onset. For instance, at $\alpha = 0^\circ$ the flow for $Re = 50$ eventually became completely steady, whereas for $Re = 55$ the final state was a flow with a stable time-dependent shedding process; see Figure 5(a). Thus in this case the onset must occur in between these two Reynolds numbers; see also Reference 16.

It follows from the linearization theory (see e.g. Reference 38) that the shedding frequency close to onset should be linear in Reynolds number, i.e. $R_0 = C_0 + C_1 Re$. At each α the frequency data were fitted to the above relationship ($Re_{cr} < Re < 65$). The critical shedding frequency was then calculated as $Ro_{cr} = C_0 + C_1 Re_{cr}$. The critical values are compiled in Table V.

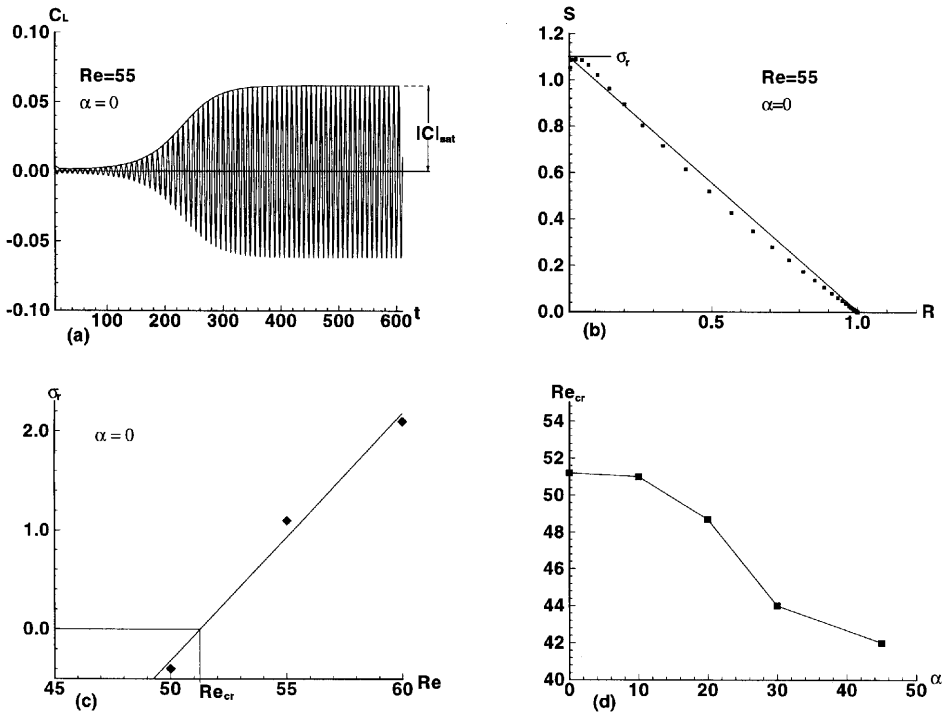

Figure 5. Onset of vortex shedding: (a) raw transient ($Re = 55, \alpha = 0^\circ$); (b) instantaneous growth rate S versus $R = |C|^2/|C|^2_{\text{sat}}$ ($Re = 55, \alpha = 0^\circ$); (c) linear global growth versus Reynolds number ($\alpha = 0^\circ$); (d) critical Reynolds number for different angles of incidence

With an increase in α from 0° to 10° the critical Re remained virtually constant ($Re_{cr} \approx 51$). At higher α, Re_{cr} showed a decrease, with a minimum value attained at $\alpha = 45^\circ$ ($Re_{\text{cr}} = 42$). It needs to be reiterated that the Reynolds number was based on the projected width. Thus at $\alpha = 45^\circ$ the critical Reynolds number based on the side dimension was about 30.

Except for the studies of Kelkar and Patankar[15] and Norberg and co-workers[8], both for zero incidence, there cannot be found in the open literature any investigation for prediction of the onset of vortex shedding for square cylinders. From a numerical linear stability analysis at a blockage β of 14·2% ($H = 7$; see Table I), Kelkar and Patankar (using an NBC) report $Re_{\text{cr}} = 53$, whereas in the practically zero-blockage experiments of Norberg and co-workers[8] the critical value is estimated to be in the range $Re_{\text{cr}} = 47 \pm 2$. As the present investigation at $\beta = 5\%$ gave $Re_{\text{cr}} = 51{\cdot}2 \pm 1{\cdot}0$, it may be conjectured that the critical Reynolds number increases with increasing blockage.

It is important to mention that on applying the present analysis to our previously calculated cases at $\alpha = 0^\circ$,[16] the critical value was $Re_{\text{cr}} = 52{\cdot}0$. In that previous investigation the far-field resolution was $\Delta = 0{\cdot}7$ using an NBC as compared with the present value of $\Delta = 0{\cdot}5$ using a CBC. Otherwise the

Table V. Calculated critical values

	$\alpha = 0^\circ$	$\alpha = 10^\circ$	$\alpha = 20^\circ$	$\alpha = 30^\circ$	$\alpha = 45^\circ$
Re_{cr}	51·2	51·0	48·7	44·0	42·0
Ro_{cr}	5·9	6·2	6·1	5·4	5·2

numerical parameters were the same. It is unclear whether this discrepancy is mostly due to the different outlet boundary condition or to the difference in Δ. Nevertheless, it may be that an even finer grid than the present one (using the CBC) could produce slightly lower critical Reynolds numbers.

4.5. *Effect of angle of incidence*

The effect of the angle of incidence ($\alpha = 0^\circ - 45^\circ$) for different Reynolds numbers ($Re = 45-200$) was investigated and results are shown in Figure 6.

When increasing the angle of incidence at different *Re*, it is worth mentioning some features in the development of a separated region at the downstream part of the body which are related to changes in

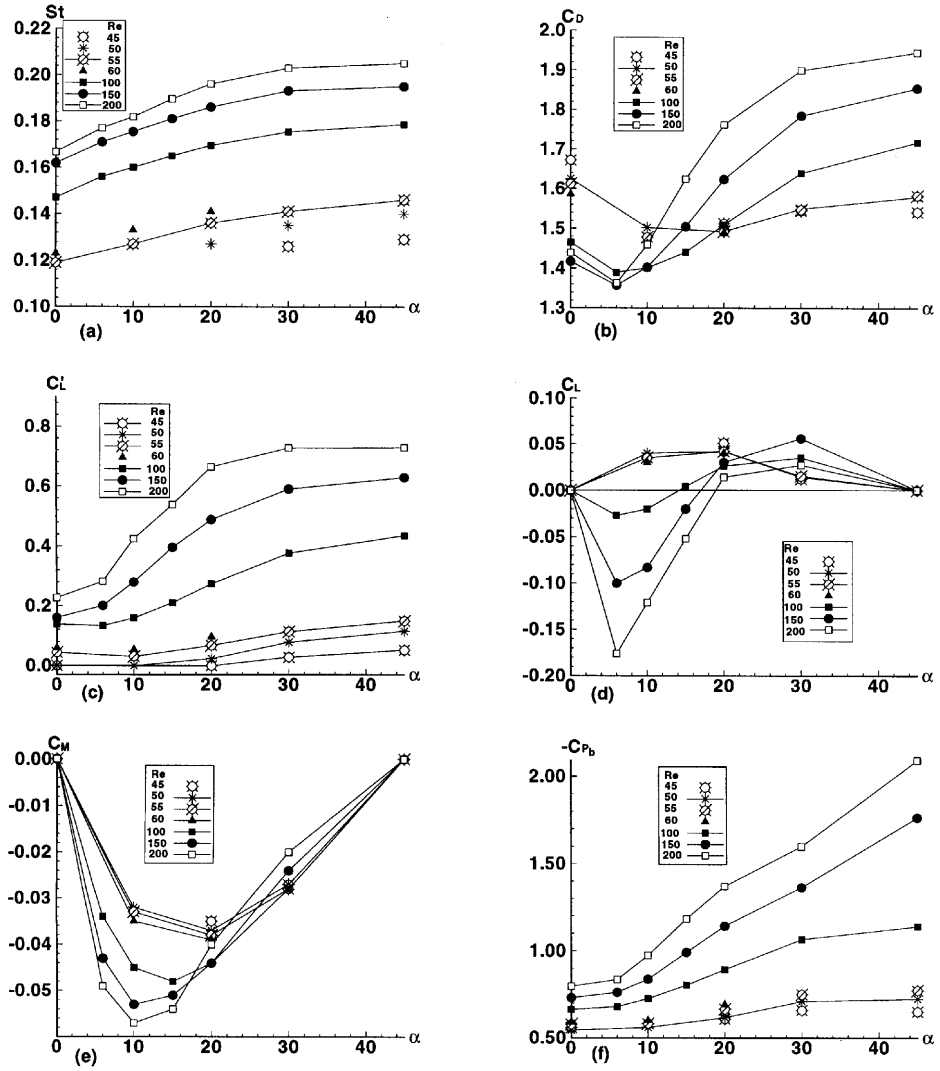

Figure 6. (a) Strouhal number (*St*), (b) drage coefficient (C_D), (c) RMS lift coefficient ($C_{L'}$), (d) lift coefficient (C_L), (e) moment coefficient (C_M) and (f) base suction coefficient) $- C_{pb}$) versus angle of incidence for different *Re*

the time mean position of the ordinary separation points. Note that the actual instantaneous separation points in some cases were actually time-dependent. During some time intervals within the shedding period and for some cases, secondary separations were also present. The following description relates to the global mean (time-averaged) fully developed shedding flow.

At $Re \leqslant 100$ and $\alpha = 0^\circ$ the separation points were located at the rear corners. Our previous investigations[8,16] show for this zero-incidence case that separation actually occur at the rear corners for $Re \leqslant 125$. However, cases at $Re = 125$ were not calculated in this study. On increasing α from zero, still for $Re \leqslant 100$, the location of the upper separation point moved upstream along the upper surface and at around $\alpha = 10^\circ - 20^\circ$ (decreasing with increasing *Re*) it reached the windward upper corner where it than remained fixed for higher α (up to $\alpha = 45^\circ$). Probably, at around $Re = 125$ this changeover occurs without a change in the angle of incidence. Within this process the lower separation point remained fixed at the rear corner. At higher Reynolds numbers ($150 \leqslant Re \leqslant 200$) and for $\alpha = 0^\circ$ the separation points were located at the upstream corners. With an increase in α the lower separation point first moved downstream on the lower surface ($\alpha < 6^\circ$) and was then located at the lower rear (leeward) corner for $\alpha \geqslant 6^\circ$. For all α within this range of Reynolds numbers the location of the upper separation point was not changed. In cases where both separation points are located at the upper and lower corners, i.e. at points defining the projected width (the diameter), the flow may be referred to as fully separated.

The Strouhal number increases smoothly on increasing the angle of incidence; see Figure 6(a). At each angle of incidence from one Reynolds number to another the value of the increase in Strouhal number is different. As can be seen in Figure 6(a), this difference between Reynolds numbers 50 and 100 is maximum and then decreases. Similar changes are also seen for the RMS lift coefficient ($C_{L'}$); see Figure 6(c) ($C_{L'}$ may be used as a measure of the vortex-shedding strength). On increasing the Reynolds number, $C_{L'}$ increases sharply and, for each angle of incidence, approximately half of these changes occur between Reynolds numbers 50 and 100.

The rates of change for *St* and $C_{L'}$ versus α (particularly for $\alpha \leqslant 20^\circ$) change sharply on increasing *Re*. As can be seen in Figure 6, for $Re = 200$ the majority of these changes occur in the range $\alpha \leqslant 20^\circ$ and then the changes are smooth. One possible reason is the occurrence of fully separated flow for higher angles of incidence.

Considering C_D versus α for different Reynolds numbers (Figure 6(b)), a local minimum on C_D curve occurs within the range $\alpha \leqslant 20^\circ$. In these low-Reynolds-number flows the changes in C_D with α are similar to those in turbulent flow, but with differences in flow pattern. The occurrence of a local minimum in C_D in turbulent flow is due to the formation of attachment points on windward surfaces, which was not observed in this range of Reynolds numbers. Possibly, for the present low *Re* this local minimum in C_D is also due to the changeover to the fully separated condition.

Figure 6(d) shows that for $Re > 100$ the mean lift coefficient has a local minimum at around $\alpha = 6^\circ$. It then increases and passes through zero lift at around $10^\circ < \alpha < 20^\circ$. For $Re < 100$, however, the lift is positive at all angles of incidence. For most cases the lift due to pressure was negative (downwards), while the lift due to friction was positive. At low *Re* the frictional lift is greater than the pressure lift, whereas the opposite behaviour was seen at higher *Re* and lower α. This causes the local minimum in lift coefficient at higher *Re*. The zero lift at around $\alpha = 10^\circ - 20^\circ$ at higher *Re* is due to a balance between frictional and pressure lift coefficients. Considering C_M versus α (Figure 6(e)), C_M reaches a minimum at approximately $\alpha = 20^\circ, 15^\circ, 10^\circ$ and 10° for $Re = 50, 100, 150$ and 200 respectively. Irrespective of the Reynolds number, however, the slope of C_M close to zero incidence is negative ($\partial C_M/\partial\alpha < 0$). As the turning moment was defined as positive in the clockwise direction, this means that the square cylinder within this range of *Re*, as also for much higher *Re*,[3] has a stable posture.

Finally, from Figure 6(f) it is seen that the base pressure coefficient increases sharply with increasing angle of incidence. The minimum and maximum differences between results for different *Re* are seen at $\alpha = 0^\circ$ and 45°. This is due to the more vigorous vortex shedding found at higher angles of incidence and for higher Re, respectively.

5. CONCLUDING REMARKS

Calculations of unsteady, incompressible 2D flow around a square cylinder at incidence and for low Reynolds numbers ($Re = 45-200$) have been carried out.

At the outlet of the computational domain a convective Sommerfeld boundary condition (CBC) is compared with a traditional Neumann condition (NBC). This comparison proves the CBC to be more effective in reducing the CPU time, reducing the upstream influence from the outlet and thus reducing the necessary downstream extent (X_d) of the domain. Within the present Reynolds number range it is recommended to use $X_d > 15$ ($X_d > 10$ for $Re = 100-200$). However, with the NBC, if X_d is sufficiently large, i.e. for $X_d > 25$ approximately, the upstream influence of the outlet is effectively damped out. In these outlet-independent cases, for both the NBC and CBC, the near-body flow patterns are virtually identical and the differences between global quantities such as Strouhal number, drag, RMS lift, etc. are negligible.

A decrease in blockage from 5% to 2·5% for $Re = 100-200$ and zero incidence resulted in a slight decrease (less than 1·5%) in Strouhal number, mean drag and RMS lift, less than a 3% increase in stagnation pressure and a maximum 8% decrease ($Re = 100$) in base suction.

For the range of Reynolds number considered, it is recommended that the cell Reynolds number (based on the far-field resolution) should be less than 30.

For the full range of possible incidences, i.e. $0^\circ \leqslant \alpha \leqslant 45^\circ$, the onset of vortex shedding occurred within the interval $40 < Re_{cr} < 55$, with a decrease in Re_{cr} with increasing α. Using a procedure based on the linearized Stuart–Landau equation, at a blockage of 5%, individual critical values at some selected incidences were calculated. For instance, at incidence $\alpha = 0^\circ$ and 45° the onset values were $Re_{cr} = 51{\cdot}2 \pm 1{\cdot}0$ and $42{\cdot}0 \pm 1{\cdot}0$ respectively.

The study also provides data on the influence of *Re* and angle of incidence on quantities such as Strouhal number and lift, drag, moment and base suction coefficients. It is found that the behaviour at low angles of incidence (particularly at $\alpha \leqslant 20^\circ$) is different from the fully separated flow at higher angles of incidence.

Experimental studies on this flow configuration for these low Reynolds numbers are very scarce. The available experiments have all been carried out for the case of zero incidence, i.e. with one side facing the oncoming flow. Nevertheless, when considering the effects of different blockages, experimental uncertainties and numerical inaccuracies, the agreement seems satisfactory. However, accurate measurements, especially at various angles of incidence, are still needed. In particular, the question of the transitional Reynolds number, i.e. the critical *Re* above which the flow ceases to be laminar and cannot be made two-dimensional, needs further investigation.

REFERENCES

1. M. Provansal, C. Mathis and L. Boyer, 'Bénard–von Kármán instability: transient and forced regimes', *J. Fluid Mech.*, **182**, 1–22 (1987).
2. C. W. Knisely, 'Strouhal numbers of rectangular cylinders at incidence: a review and new data', *J. Fluids Struct.*, **4**, 371–393 (1990).
3. C. Norberg, 'Flow around rectangular cylinders: pressure forces and wake frequencies', *J. Wind Engng. Ind. Aerodyn.*, **49**, 187–196 (1993).
4. A. Okajima, 'Strouhal numbers of rectangular cylinders', *J. Fluid Mech.*, **123**, 379–398 (1982).

5. R. W. Davis and E. F. Moore, 'A numerical study of vortex shedding from rectangles', *J. Fluid Mech.*, **116**, 475–506 (1982).
6. A. Okajima, T. Nagahisa and A. Rokugoh, 'A numerical analysis of flow around rectangular cylinders', *JSME Int. J. Ser. II*, **33**, 702–711 (1990).
7. A. Okajima, 'Numerical analysis of the flow around an oscillating cylinder', *Proc. 6th Int. Conf. on Flow-Induced Vibration*, London, 1995.
8. A. Sohankar, C. Norberg and L. Davidson, 'Numerical simulation of unsteady low-Reynolds number flow around a rectangular cylinder at incidence', *Proc. 3rd Int. Colloq. on Bluff Body Aerodynamics and Applications*, VA, 1996.
9. T. G. Zaki, M. Sen and M. Gad-El-Hak, 'Numerical and experimental investigation of flow past a freely rotational square cylinder', *J. Fluids Struct.*, **8**, 555 (1994).
10. N. Stegell and N. Rockliff, 'Simulation of the effects of body shape on lock-in characteristics in pulsating flow by the discrete vortex method', *Proc. 3rd Int. Colloq. on Bluff Body Aerodynamics and Applications*, VA, 1996.
11. H. Suzuki and Y. Inoue, 'Unsteady flow in a channel obstructed by a square rod (crisscross motion of vortex)', *Int. J. Heat Fluid Flow*, **14**, 2–9 (1993).
12. G. Li and J. A. C. Humphrey, 'Numerical modeling of confined flow past a cylinder of square cross-section at various orientations', *Int. j. numer. meth. fluids*, **20**, 1215–1236 (1995).
13. R. Franke, W. Rodi and B. Schönung, 'Numerical calculation of laminar vortex-shedding flow past cylinders', *J. Wind Engng. Ind. Aerodyn.*, **35**, 237–257 (1990).
14. M. P. Arnal, D. J. Goering and J. A. C. Humphrey, 'Vortex shedding from a bluff body adjacent to a plane sliding wall', *J. Fluids Engng., Trans. ASME*, **113**, 384–398 (1991).
15. K. M. Kelkar and S. V. Patankar, 'Numerical prediction of vortex shedding behind a square cylinder', *Int. j. numer. meth. fluids*, **14**, 327 (1992).
16. A. Sohankar, L. Davidson and C. Norberg, 'Numerical simulation of unsteady flow around a square two-dimensional cylinder', *Proc. Twelfth Australasian Fluid Mechanics Conf.*, Sydney, 1995, pp. 517–520.
17. T. Yoshida, T. Watanabe and I. Nakamura, 'Numerical anlaysis of open boundary conditions for incompressible viscous flow past a square cylinder', *Trans. JSME*, **59**2799–2806 (1993).
18. A. Okajima and K. Sugitani, 'Flows around rectangular cylinders. Numerical calculations and experiments. Part 2', *Bull Res. Inst. Appl. Mech., Kyushu Univ.*, (1979).
19. A. Okajima, A. Rokugou and H. Ueno, 'Calculation program of laminar flow around a rectangular cylinder by finite difference methods', *Tech. Rep.*, Faculty of Technology, Kanazawa University, 1987.
20. P. K. Stansby and A. Slaouti, 'Simulation of vortex shedding including blockage by the random-vortex and other methods', *Int. j. numer meth. fluids*, **17**, 1003–1013 (1993).
21. P. Anagnostopoulos, G. Illiadis and S. Richardson, 'Numerical study of the blockage effects on viscous flow past a circular cylinder', *Int. j. numer. meth. fluids*, **22**, 1061–1074 (1996).
22. M. Behr, D. Hastretier, S. Mittal and T. E. Tezduyar, 'Incompressible flow past a circular cylinder: dependence of the computed flow field on the location of the lateral boundaries', *Comput. Meth. Appl. Mech. Engng.*, **123**, 309–316 (1995).
23. H. B. Awbi, 'Wind-tunnel-wall constraint on two-dimensional rectangular-section prisms', *J. Ind. Aerodyn.*, **3**, 285–306 (1978).
24. H. B. Awbi, 'Effect of blockage on the Strouhal number of 2D bluff bodies', *J. Wind Engng. Ind. Aerodyn.*, **12**, 353–363 (1983).
25. J. M. Chen and Y. Fang, 'Strouhal numbers of inclined plates', *J. Wind Engng. Ind. Aerodyn.*, **61**, 99–112 (1996).
26. M. Behr, J. Liou, R. Shih and T. E. Tezduyar, 'Vorticity–streamfunction formulation of unsteady incompressible flow past a cylinder: sensitivity fo the computed flow field to the location of the outflow boundary', *Int. j. numer meth. fluids*, **12**, 323–342 (1991).
27. H. Le and P. Moin, 'Direct numerical simulation of turbulent flow over a backward facing step', *Rep. TF-58*, Department of Mechanical Engineering, Stanford University, 1994.
28. H. Zhang, U. Fey and B. Noack, 'On the transition of the cylinder wake', *Phys. Fluids*, **7**, 779–794 (1995).
29. I. Orlanski, 'A simple boundary condition for unbounded hyperbolic flows', *J. Comput. Phys.*, **21**, 251–269 (1976).
30. D. H. Rudy, 'A nonreflecting outflow boundary condition for subsonic Navier–Stokes calculation', *J. Comput. Phys.*, **36**, 55–70 (1980).
31. T. Y. Han, J. C. S. Meng and G. E. Innis, 'An open boundary condition for incompressible stratified flows', *J. Comput. Phys.*, **49**, 276–297 (1983).
32. Ch. H. Bruneau and P. Fabrie, 'Effective downstream boundary conditions for incompressible Navier–Stokes equations', *Int. j. numer. meth. fluids*, **19**, 693–705 (1994).
33. R. L. Sani and P. M. Gresho, 'Resume and remarks on the open boundary condition minisymposium', *Int. j. numer. meth. fluids*, **18**, 983–1008 (1994).
34. H. Han and W. Bao, 'An artificial boundary condition for 2-D incompressible viscous flows using the method of lines', *Int. j. numer. meth. fluids*, **22**, 483–493 (1996).
35. J. Heywood, R. Rannacher and S. Turek, 'Artificial boundary and flux and pressure conditions for the incompressible Navier–Stokes equations', *Int. j. numer. meth. fluids*, **22**, 325–352 (1996).
36. L. Pauley, P. Moin and W. C. Reynolds, 'The structure of two-dimensional separation', *J. Fluid Mech.*, **220**, 397–411 (1990).
37. C. P. Jackson, 'A finite-element study of the onset of vortex shedding in flow past variously shaped bodies', *J. Fluid Mech.*, **182**, 23–45 (1987).

38. M. Schumm, E. Berger and P. A. Monkewitz, 'Self-excited oscillations in the wakes of 2-D bluff bodies and their control', *J. Fluid Mech.*, **271**, 17–53 (1994).
39. D. S. Park, 'Theoretical analysis of feedback control of Kármán vortex shedding at slightly supercritical Reynolds numbers', *Eur. J. Mech. B/Fluids*, **13**, 387–399 (1994).
40. X. Yang and A. Zebib, 'Absolute and convective instability of a cylinder wake', *Phys. Fluids A*, **1**, 689–696 (1989).
41. B. R. Noack and H. Eckelmann, 'A global stability analysis of the steady and periodic cylinder wake', *J. Fluid Mech.*, **270**, 297–330 (1994).
42. M. Nishioka and H. Sato, 'Mechanism of determination of the shedding frequency of vortices behind a cylinder at low Reynolds numbers', *J. Fluid Mech.*, **89**, 49–60 (1978).

